Modelling and DEM simulations of toner behavior in a print process

Modelling and DEM simulations of toner behavior in a print process

I.E.M. Severens[1], R.M.M. Mattheij[2], A.A.F. van de Ven[2], D.E. Wolf[3]

[1] Océ Technologies B.V., Venlo, the Netherlands
[2] Department of Mathematics, Eindhoven University of Technology, Eindhoven, the Netherlands
[3] Department of Physics, Gerhard Mercator Universität, Duisburg, Germany

Abstract This paper describes the modeling of the toner behavior in the development nip of the Océ Direct Imaging print process. The dynamic motion of and mechanical interactions between toner particles are explicitly modelled. The mechanical interactions are due to collisions, friction, adhesion, and electromagnetic forces. The discrete element method (DEM) is used as the simulation tool for a quantitative description of the system. The interaction rules are determined for the toner particles and the surfaces of the development rollers. The model is validated with print quality results. It is shown that it is possible to achieve quantitative agreement between DEM simulations and experimental print quality results.

1 Introduction

The heart of the Océ Direct Imaging (DI) print process is formed by the Direct Imaging unit, which is schematically shown in Figure 1. For a more detailed description of the DI print process, we refer to [1].

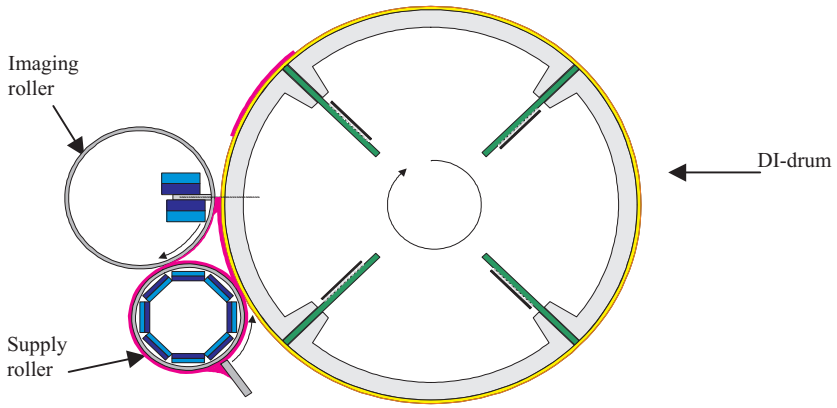

Figure1. Schematic drawing of the Direct Imaging process.

The toner that is used in this development process is mono-component, magnetizable, and electrically conductive. Toner is magnetically drawn towards a supply roller, which conveys the toner particles through friction. As a result of a bias voltage between the supply roller and the DI-drum, attraction of toner towards the DI-drum is achieved by induced electrostatic forces. The toner layers that are attracted onto the DI-drum move along with the DI-drum until they reach the fixed magnet that is placed underneath the imaging roller. The fixed magnet within the imaging roller causes a strong magnetic field gradient, attracting the

magnetic toner particles towards the imaging roller. By choosing the geometry of the magnet properly, a sharp cut-off of the field gradient can be achieved, providing a precise control over the position of the toner between the DI-drum and the imaging roller. If an image is to be developed, a voltage is applied to the DI-drum and the toner is drawn to the DI-drum.

The print quality of the Direct Imaging technology is primarily determined by the toner flow in the region between the DI-drum and the imaging roller; see Figure 2. The collection

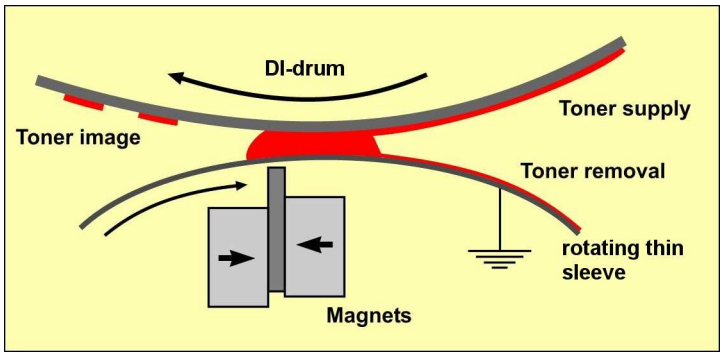

Figure2. The collection of toner between the DI-drum and the imaging roller.

of toner between the DI-drum and the imaging roller is called the DI toner assembly. The behavior of the DI toner assembly is determined by magnetic, electric, and mechanical forces. The sum of these forces results in a complex system behavior; see [2]. Insight in the underlying physical processes of Direct Imaging can be obtained by experimental research. The possibilities of experimental characterization of the DI toner assembly are, however, limited. This is essentially caused by the small dimensions of the system.

Another approach to get insight in the toner flow in the DI-unit is theoretical modeling and numerical simulation. The simulation of toner deposition, conducted here, consists of a many-body system, where the motion of each particle is calculated knowing the forces acting on it. This method employs the discrete element method, first proposed by Cundall [3] in 1971. In the discrete element method (DEM), all toner particles are considered discrete elements. Each element interacts with its neighboring elements and its surroundings. Every time step, the forces that act on a particle are summed and, from this, the speed and the displacement of the particle is calculated by integration of Newton's second law of motion. The macroscopic behavior of the toner flow and print output can thus be simulated using DEM.

The modeling of the geometry of the toner particles is described in Section 2. A two-dimensional model is developed. However, the models for the forces that act on the toner particles in the DI assembly are three-dimensional. The dominant forces in the DI toner assembly are normal and tangential collision forces between particles themselves and between particles and developing rollers, adhesive and cohesive forces, magnetic forces on toner particles due to the magnet within the imaging roller and due to the presence of magnetized particles, and electric forces between particles and the DI-drum. Models for these forces are derived and discussed in Sections 3 to 6. In Section 7, we analyze to what extent we have succeeded in describing the DI print process.

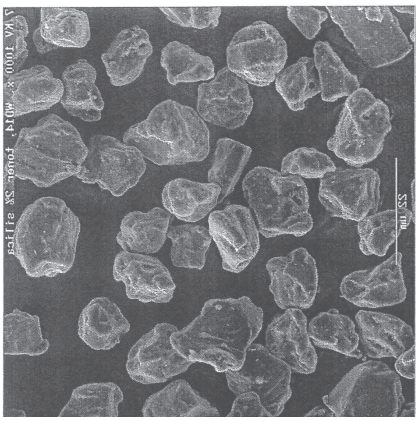

Figure3. SEM recording of black toner particles.

2 Geometry of the DI toner assembly

In Figure 3, a scanning-electron-microscopy (SEM) recording of a collection of black toner particles is depicted. Since modeling of complex geometries, as shown in Figure 3, results in time-consuming algorithms, one often confines oneself to simple geometrical shapes, such as spheres. Spherical particles can, however, role frictionless over a surface or over each other. Real toner particles cannot show this rolling behavior due to their geometry. To resolve this limitation of the single-sphere model, a model is used in which n spherical particles ($n = 1, 2, ...$) are kinematically clustered, according to a predefined distance between the centers of the spheres. For $n = 2$, a holonomic constraint is defined between sphere i and sphere j at respective positions $\mathbf{x}_i$, $\mathbf{x}_j$, namely

$$|\mathbf{x}_i - \mathbf{x}_j| = l, \tag{2.1}$$

with l a predefined distance. One toner particle is thus described by n clustered spheres, as can be seen in Figure 4. More realistic toner geometries can thus be achieved by increasing

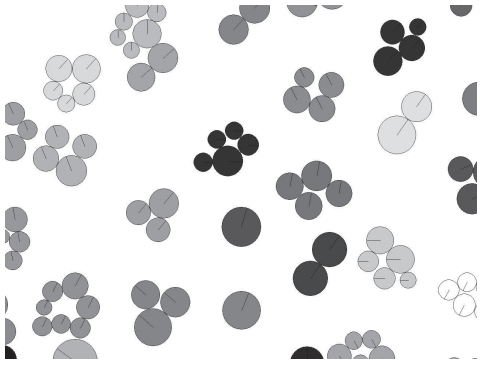

Figure4. Kinematically clustered spheres form one toner particle.

the number of clustered spheres that form one toner particle; this, however, has its impact on computational speed.

3 Force model for collisions

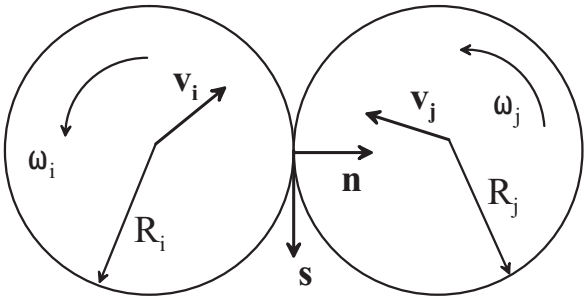

Figure5. Collision between two particles i and j.

In this section, the forces due to collisions between two particles or a particle and a boundary object are modeled. The DEM variant used here is, sometimes, referred to as the soft-particle method [4,5]. This means that the collision is modeled by penetration of the objects during collision. We here consider only collisions that take place in one plane (2-D collisions). The toner particles are modeled as spheres (or circular discs in the 2-D plane); the i-th particle having mass m_i and radius R_i. The particles are only locally modeled as discs; globally, they consist of more clustered discs, but this is for the moment not relevant here. A solid boundary is modeled as a particle by letting m_i and R_i go to infinity. The position of the center of mass of the i-th particle in the plane is $\mathbf{x}_i = \mathbf{x}_i(t)$ ($\mathbf{x}_i \in \mathbb{R}^2$), and its velocity is $\mathbf{v}_i = \dot{\mathbf{x}}_i(t)$. The particles (discs) also have angular velocity, directed normal to the plane and of magnitude ω_i for the i-th particle. For the nomenclature as used in the rest of this section, consider the collision between two particles i and j, as depicted in Figure 5.

We split the velocity $\mathbf{v}_i$ in its normal and tangential component according to ($\mathbf{n}$ and $\mathbf{s}$ as in Figure 5)

$$\mathbf{v}_i = v_{i,n}\mathbf{n} + v_{i,s}\mathbf{s}, \tag{3.1}$$

and we introduce the relative normal and tangential velocity v_n and v_s, respectively, of the contact points for a collision between two particles i and j, by

$$v_n = v_{j,n} - v_{i,n}, \tag{3.2}$$

and

$$v_s = v_{j,s} - v_{i,s} + \omega_i R_i + \omega_j R_j. \tag{3.3}$$

3.1 Normal collision

For a pure normal collision, the velocities of the two colliding particles are directed along the normal $\mathbf{n}$ on the contact surface at collision. According to the soft-particle model, the (elastic) particles deform during the collision, modeled as a penetration of the objects into each other. The overlap ξ during this penetration is equal to

$$\xi = R_i + R_j - |\mathbf{x}_i - \mathbf{x}_j|. \tag{3.4}$$

A range of possible contact force models are available, each approximating the collision dynamics to some extent; see [1] or [2]. Here, we restrict ourselves to the linear model

$$F_n = -k\xi - \gamma\frac{d\xi}{dt}\ , \tag{3.5}$$

where F_n is the normal force between the colliding particles during the collision. The first term on the right-hand side is the elastic restoring force and the second term describes viscoelastic dissipation [6]. The material constants k and γ are the elastic spring constant and the viscous damping coefficient, respectively.

The integration scheme that is used to solve the collisions is Newmark's purely explicit method

$$\begin{aligned} x_{n+1} &= x_n + \Delta t v_n + \frac{1}{2}\Delta t^2 F_n, \\ v_{n+1} &= v_n + \Delta t F_n. \end{aligned} \tag{3.6}$$

Newmark purely explicit is a first-order method. Substitution of $F = (-kx - \gamma\dot{x})/m$ in (3.6) gives

$$\begin{aligned} x_{n+1} &= (1 - \tfrac{k}{2m}\Delta t^2)x_n + \Delta t(1 - \tfrac{\gamma}{2m}\Delta t)v_n, \\ v_{n+1} &= -\tfrac{k}{m}\Delta t x_n + (1 - \tfrac{\gamma}{m}\Delta t)v_n. \end{aligned} \tag{3.7}$$

Substitution of $(3.7)^2$ in $(3.7)^1$ with index n replaced by $n+1$, and substitution of

$$\Delta t(1 - \frac{\gamma}{2m}\Delta t)v_n = x_{n+1} - (1 - \frac{k}{2m}\Delta t^2)x_n \tag{3.8}$$

gives

$$x_{n+2} = (2 - \frac{k}{2m}\Delta t^2 - \frac{\gamma}{m}\Delta t)x_{n+1} - (1 + \frac{k}{2m}\Delta t^2 - \frac{\gamma}{m}\Delta t)x_n. \tag{3.9}$$

After defining k^* and γ^* as

$$k^* := \frac{k}{2m}\Delta t^2, \qquad \gamma^* := \frac{\gamma}{m}\Delta t, \tag{3.10}$$

(3.9) can be written as

$$x_{n+1} + (-2 + k^* + \gamma^*)x_n + (1 + k^* - \gamma^*)x_{n-1} = 0. \tag{3.11}$$

In order to analyze the stability of this scheme, the discrete Fourier mode

$$x_n = \lambda^n, \tag{3.12}$$

is substituted in (3.11). This way, we obtain for the amplification factor λ:

$$\lambda_{1,2} = \frac{2 - k^* - \gamma^* \pm \sqrt{(k^* + \gamma^*)^2 - 8k^*}}{2}. \tag{3.13}$$

Extensive analysis of the properties of the amplification factors $\lambda_{1,2}$ shows that Newmark purely explicit is stable if

$$\gamma^* \geq k^*, \qquad \text{and} \qquad \gamma^* \leq 2. \tag{3.14}$$

Substitution of (3.10) in (3.14) shows that for $\Delta t \leq \min\{2m/\gamma, 2\gamma/k\}$ Newmark purely explicit is (conditionally) stable.

The normal dissipation in a collision is characterized by the coefficient of normal restitution, which is defined as the ratio between the normal component of the relative velocity before $v_n^{(i)}$ and after $v_n^{(f)}$ the collision,

$$e_n = |v_n^{(f)}/v_n^{(i)}|. \tag{3.15}$$

This coefficient varies between 0 for completely inelastic and 1 for perfectly elastic collisions (no normal dissipation). The effective normal coefficient of restitution and the collision duration time t_n can be expressed in terms of the collision parameters k and γ, namely (see [2])

$$e_n = \exp\left(-\frac{\pi}{\omega}\right), \qquad t_n = \frac{m\pi}{\gamma\omega}, \tag{3.16}$$

with ω and m given by

$$\omega = \frac{1}{2}\sqrt{\frac{4mk}{\gamma^2} - 1}, \qquad m = \frac{m_1 m_2}{m_1 + m_2}. \tag{3.17}$$

For our applications, we determine e_n and t_n experimentally (see [1] or [7]) and from the results, we can then calculate k and γ. The thus obtained values will be used in our DEM simulations.

3.2 Tangential collision

Collisions amongst particles or between particles and objects are, in general, not head-on, and thus, shear also has to be taken into account. The shear contact force component F_s, being the component in **s**-direction of the contact force on particle i, is generally modeled with a Coulomb friction model:

$$\begin{aligned} F_s &= -\mu_d F_n \text{sign}(v_s), && v_s \neq 0, \\ |F_s| &< \mu_s F_n, && v_s = 0, \end{aligned} \tag{3.18}$$

where μ_s is the coefficient of static friction, F_n the normal force at the contact ($F_n > 0$ always), v_s the relative tangential velocity of the two particles as defined in (3.3), and μ_d the coefficient of dynamic friction ($\mu_d < \mu_s$). The Coulomb law is discontinuous at zero velocity. Since Coulomb friction is a discontinuous force model, adjustments have to be made to the model to avoid numerical instability of the force law in a simulation.

A simple implementation of the shear contact force is found in [4]. In this paper, Cundall and Strack modeled the shear contact force by an incrementing spring, which accounts for tangential elastic deformation of the contacting surfaces, according to

$$F_s = -k_s \eta, \tag{3.19}$$

where k_s is the spring constant of the spring, which from time t_0 on, at which the contact was first established, has been stretched over a distance η given by

$$\eta = \int_{t_0}^{t} v_s(\tau) d\tau. \tag{3.20}$$

The tangential spring causes an oscillatory motion around the point $\eta = 0$. The tangential spring force is limited by the maximal static Coulomb friction $\mu_s F_n$; this is the limiting friction that can be withstood by the contact before sliding of one particle over the other commences. In case of sliding, the shear contact force is given by kinetic Coulomb friction $\mu_d F_n$. From that point on, the spring is not stretched further. Since the friction force acts on the surface of the particle, also a moment M is exerted on the particle according to

$$M = RF_s, \tag{3.21}$$

with R the distance from the center of mass of the particle i to the contact point.

4 Adhesion force

When two materials are brought into each others vicinity, they exert an attracting force onto each other, the adhesion force. Hamaker [8] derived the following expression for the attractive force between two spherical bodies with radii R_1 and R_2 as a function of the distance d:

$$F_{adh} = \frac{AR_1R_2}{12(R_1 + R_2)d^2}, \tag{4.1}$$

where A is known as the Hamaker coefficient. The Hamaker coefficient is a material property. The expression (4.1) is employed in this paper for the calculation of adhesive forces; for d we take the distance between the centers of the spherical particles. Accordingly, the adhesion force in the model increases linearly with the particle size R and is inversely proportional to d^2.

5 Magnetic force

Toner particles contain magnetic pigment particles, which are magnetizable in an external magnetic field. A magnetic particle in a non-uniform magnetic field, just as a magnetic particle in the neighborhood of another magnetic particle, experiences a magnetic force. In this section, we present force models for the magnetic forces that act on and between toner particles in the DI toner assembly.

In a magnetostatic problem, the field vectors in $\mathbf{x} \in \mathbb{R}^3$ satisfy the system

$$\nabla \times \mathbf{H} = \mathbf{J}, \qquad \nabla \cdot \mathbf{B} = 0, \tag{5.1}$$

with $\mathbf{H}$ the magnetic field, $\mathbf{J}$ the current density and $\mathbf{B}$ the magnetic flux. In fact, this also holds for a dynamic situation if the electric quasi-static approximation may be applied. This approximation holds for relatively slow process, i.e. slow with respect to the speed of light, and it amounts to the neglect of the displacement current $\partial \mathbf{D}/\partial t$ with respect to $\mathbf{J}$, or $\nabla \times \mathbf{H}$. According to $(5.1)_2$, the field of the vector $\mathbf{B}$ is always solenoidal. Consequently, $\mathbf{B}$ can be represented as the curl of another vector $\mathbf{A}(\mathbf{x})$, the magnetic vector potential,

$$\mathbf{B}(\mathbf{x}) = \nabla \times \mathbf{A}(\mathbf{x}). \tag{5.2}$$

The magnetic vector potential $\mathbf{A}(\mathbf{x})$ in a point $\mathbf{x}$ external to a conducting body $\mathcal{B}$, of configuration $G \in \mathbb{R}^3$, is then given by the well-known formula (see [9, p.235])

$$\mathbf{A}(\mathbf{x}) = \frac{\mu}{4\pi} \int_G \frac{\mathbf{J}(\mathbf{x}')}{|\mathbf{x} - \mathbf{x}'|} d\tau_{x'} \ . \tag{5.3}$$

A general current distribution localized in a small region of space is now considered; "small" being relative to the scale of length of interest to the observer. It will be assumed that the entire distribution can be circumscribed by a sphere B of finite radius R drawn from the origin; only points of observation $\mathbf{x}$ exterior to this sphere will be considered. Vector calculations show that

$$\frac{1}{|\mathbf{x}-\mathbf{x}'|} = \frac{1}{\sqrt{|\mathbf{x}|^2 - 2|\mathbf{x}||\mathbf{x}'|\cos\theta + |\mathbf{x}'|^2}}, \tag{5.4}$$

with θ the angle between the vectors $\mathbf{x}$ and $\mathbf{x}'$. Assuming $|\mathbf{x}| > |\mathbf{x}'|$, the denominator on the right-hand side of (5.4) can be expanded in powers of $|\mathbf{x}'|/|\mathbf{x}|$, measured relative to the origin, thus giving

$$\frac{1}{|\mathbf{x}-\mathbf{x}'|} = \frac{1}{|\mathbf{x}|}\sum_{n=0}^{\infty} P_n(\cos\theta)\left(\frac{|\mathbf{x}'|}{|\mathbf{x}|}\right)^n, \tag{5.5}$$

with P_n a Legendre polynomial of order n, [10]. Substitution of (5.5) into (5.3), making use of (the first condition is necessary to exclude magnetic monopoles; see [11])

$$\int_B \mathbf{J}(\mathbf{x}')\tau_{x'} = \mathbf{0}, \qquad \nabla\cdot\mathbf{J} = 0, \tag{5.6}$$

and leaving out all second-order terms, gives

$$\mathbf{A}(\mathbf{x}) = -\frac{\mu}{8\pi|\mathbf{x}|^3}\left[\mathbf{x}\times\int_B \mathbf{x}'\times\mathbf{J}(\mathbf{x}')d\tau_{x'}\right]. \tag{5.7}$$

It is customary to define the magnetic moment density or magnetization $\mathbf{M}$ as

$$\mathbf{M}(\mathbf{x}) = \frac{1}{2}\,\mathbf{x}\times\mathbf{J}(\mathbf{x}), \tag{5.8}$$

and its integral over G as the magnetic moment $\mathbf{m}$ as

$$\mathbf{m} = \frac{1}{2}\int_G \mathbf{x}'\times\mathbf{J}(\mathbf{x}')d\tau_{x'}. \tag{5.9}$$

Then, the first-order term of the vector potential is the magnetic dipole vector potential,

$$\mathbf{A}(\mathbf{x}) = \frac{\mu}{4\pi}\frac{\mathbf{m}\times\mathbf{x}}{|\mathbf{x}|^3}\ . \tag{5.10}$$

The magnetic flux $\mathbf{B}$ outside the localized source can be calculated directly by evaluating the curl of (5.10), leading to

$$\mathbf{B}(\mathbf{x}) = \frac{\mu}{4\pi}\left[\frac{3(\mathbf{e}_r\cdot\mathbf{m})\mathbf{e}_r - \mathbf{m}}{|\mathbf{x}|^3}\right]. \tag{5.11}$$

Here, $\mathbf{e}_r$ is a unit vector in the direction of $\mathbf{x}$.

If a localized distribution of current is placed in an external magnetic flux field $\mathbf{B}(\mathbf{x})$, it experiences a Lorentz force. The general expression for the total force $\mathbf{F}$ is

$$\mathbf{F} = \int_G \mathbf{J}(\mathbf{x}')\times\mathbf{B}(\mathbf{x}')d\tau_{x'}. \tag{5.12}$$

If the external magnetic flux varies slowly over the region of current, a Taylor series expansion can be utilized to find the dominant terms in the force. A component k of $\mathbf{B}$ can be expanded around a suitable fixed point $\mathbf{x}$,

$$B_k(\mathbf{x}') = B_k(\mathbf{x}) + (\mathbf{x}' - \mathbf{x}) \cdot \nabla B_k(\mathbf{x}) + ..., \qquad \mathbf{x}, \mathbf{x}' \in G. \tag{5.13}$$

With this, the force (5.12) can be expressed in terms of $\mathbf{m}$ and $\mathbf{B}$, yielding

$$\mathbf{F} = (\mathbf{m} \times \nabla) \times \mathbf{B} = \nabla(\mathbf{m} \cdot \mathbf{B}) - \mathbf{m}(\nabla \cdot \mathbf{B}). \tag{5.14}$$

Since $\nabla \cdot \mathbf{B} = 0$, the lowest order force on a localized current distribution in an external magnetic field $\mathbf{B}$ is

$$\mathbf{F} = \nabla(\mathbf{m} \cdot \mathbf{B}). \tag{5.15}$$

In the quasi-static approximation, $\nabla \times \mathbf{B} = \mathbf{0}$ holds outside the source of the magnetic flux. Then, the force (5.15) can be expressed alternatively as

$$\mathbf{F}_{\text{mag}} \equiv \mathbf{F} = (\mathbf{m} \cdot \nabla)\mathbf{B}. \tag{5.16}$$

It is this formula that is used in the rest of this paper and in the numerical simulations for the magnetic (Lorentz) force.

Toner particles get their magnetic properties from the magnetic pigment particles, which are mixed with the resin of the toner. The magnetic pigment particles in the toner are not permanent magnetic particles, but they are magnetizable in an external magnetic field, according to a hysteresis curve. The magnetization $\mathbf{m}$ of a pigment particle thus depends on the external magnetic field. The magnetic field in a toner particle in the DI toner assembly originates from two sources: the fixed magnet within the imaging roller, causing a field $\mathbf{B}_m$, and the magnetized surrounding particles, resulting in a field $\mathbf{B}_a$. So, using the general formula $\mathbf{F}_{\text{mag}} = (\mathbf{m} \cdot \nabla)\mathbf{B}$, we can write here for the total magnetic force on a toner particle

$$\mathbf{F}_{\text{mag}} = (\mathbf{m} \cdot \nabla)(\mathbf{B}_m + \mathbf{B}_a), \tag{5.17}$$

where $\mathbf{m}$ is the total magnetic moment in the toner particle due to $\mathbf{B}_m + \mathbf{B}_a$ (so, $\mathbf{m} = \mathbf{m}(\mathbf{B}_m + \mathbf{B}_a)$). Accordingly, the force (5.17) can be split into two terms

$$\mathbf{F}_{\text{mag}} = \mathbf{F}_m + \mathbf{F}_a, \tag{5.18}$$

where

$$\mathbf{F}_m = (\mathbf{m} \cdot \nabla)\mathbf{B}_m, \tag{5.19}$$

represents the magnetic force exerted by the magnet within the imaging roller on the toner particle, while

$$\mathbf{F}_a = (\mathbf{m} \cdot \nabla)\mathbf{B}_a = \sum_{j \neq i} (\mathbf{m} \cdot \nabla)\mathbf{B}_j, \tag{5.20}$$

represents the magnetic force exerted by the DI toner assembly on the toner particle i. Here, $\mathbf{B}_j$ is the magnetic field due to another toner particle j, $j \neq i$, and the gradient $\nabla \mathbf{B}_j$ should be evaluated in the point $\mathbf{x}$ of particle i. Both forces are analyzed further in this section.

One black toner particle contains about 20,000 magnetic pigment particles, and one color toner particle contains on average 13 pigment particles. It will be clear that calculating the magnetic force on all magnetic pigment particles in one toner particle by evaluation of (5.19) is computationally not achievable. If we assume that the magnetic field gradient $\nabla \mathbf{B}_m$ does not vary over a toner particle, then the force (5.19) on one toner particle can be written as

$$\mathbf{F}_m = (\sum_{k=0}^{K} \mathbf{m}_k \cdot \nabla)\mathbf{B}_m = (\mathbf{m} \cdot \nabla)\mathbf{B}_m, \tag{5.21}$$

with

$$\mathbf{m} = \sum_{k=0}^{K} \mathbf{m}_k, \tag{5.22}$$

the total magnetic moment of the toner particle and K the number of pigment particles in that toner particle.

The magnetic field $\mathbf{B}_m$ of the magnet within the imaging roller is calculated with Flux2D [12]. Flux2D is a software package, based on the finite element method (FEM), for the analysis and design of electromagnetic and electromechanical devices and processes. By defining the geometry, the magnetic properties, e.g. the magnetization curves of the different materials used in the construction of the magnet, and the properties of the FEM mesh, the magnetic field is calculated in a predefined area of interest. The result, see Figure 6, is used as input for our magnetic force calculations.

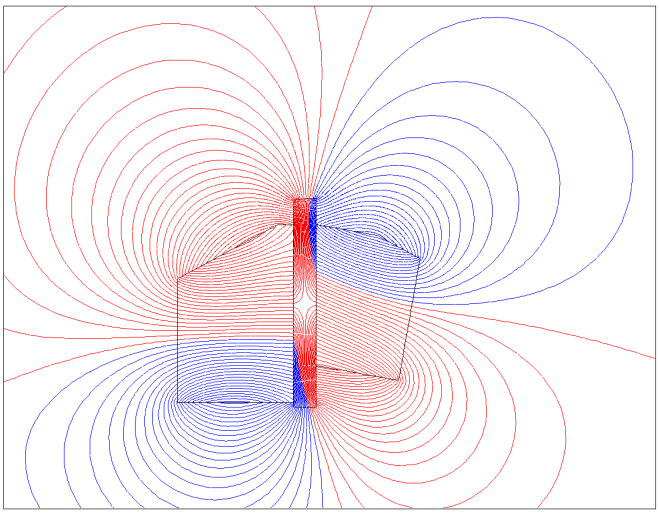

Figure6. Magnetic field calculations with Flux2D. The magnetic field lines for the magnetic knife are visualized.

To evaluate (5.20), we note that the magnetic field at position $\mathbf{x}$ caused by a magnetic dipole $\mathbf{m}_j$ at position $\mathbf{x}_j$ is given by

$$\mathbf{B}_j(\mathbf{x}) = \frac{\mu_0}{4\pi}\left(\frac{3(\mathbf{x}-\mathbf{x}_j)\mathbf{m}_j \cdot (\mathbf{x}-\mathbf{x}_j)}{|\mathbf{x}-\mathbf{x}_j|^5} - \frac{\mathbf{m}_j}{|\mathbf{x}-\mathbf{x}_j|^3}\right). \tag{5.23}$$

The force exerted on a magnetic dipole $\mathbf{m}_i$ in $\mathbf{x} = \mathbf{x}_i$ by the external magnetic field $\mathbf{B}_a$ is then, according to (5.20), given by

$$\mathbf{F}_a(\mathbf{x}_i) = \sum_{j \neq i} (\mathbf{m}_i \cdot \nabla)\mathbf{B}_j(\mathbf{x}_i). \tag{5.24}$$

6 Electric force

In this section, we derive a model for the electric force acting on particles in the DI toner assembly, and a model that quantifies the dynamic charging and decharging of the DI toner assembly. For this, we consider the configuration for the front region of the DI toner assembly depicted in Figure 7; see also this figure for the meaning of G_i and C_i. The region in front of the toner assembly (air or vacuum) is denoted by G_1. The imaging roller, C_d, is grounded, so at the surface of the imaging roller the electric potential is zero. The toner particles, $G_3, G_4, ..., G_n$, are connected via a conducting path with the imaging roller, and thus also have zero potential. The drum, C_u, is put on a voltage V, which is alternatively 0 or 40 Volt. The drum is coated with a dielectric layer, G_2 made of SiO_x, with a relative dielectric permeability ε_2 of 5, and a thickness d_l of 600nm. Finally, far away from the front, C_l(left) or C_r(right), it is assumed that the electric field is perpendicular to the DI-drum and to the imaging roller.

To enable electric field transfer, the electric force exerted by the externally applied electric field on the toner particle must be stronger than the magnetic force. The electrostatic force $\mathbf{F}$, the Coulomb force, on a charged body of configuration G ($G \subset \mathbb{R}^3$) is equal to

$$\mathbf{F} = \int_G \sigma(\mathbf{x})\mathbf{E}(\mathbf{x}) d\tau, \tag{6.1}$$

where $\mathbf{E}$ is the electric field strength and σ the volume charge density in the body.
In the non-conducting space $G_1 \cup G_2$ outside the spheres, where there is no free charge, the electric field strength satisfies

$$\nabla \cdot \mathbf{D} = \varepsilon \nabla \cdot \mathbf{E} = 0, \tag{6.2}$$

where ε is ε_0 in G_1, and $\varepsilon_0\varepsilon_2$ in G_2.
If an electric potential u is introduced by $\mathbf{E} = -\nabla u$, then, according to (6.2), u is a solution of the Laplace equation. Moreover, $u = 0$ in $G_3 \cup G_4 \cup .... \cup G_n$. In summary, the following problem can be formulated:
find $u_1, u_2, u_3, ..., u_n$, such that the following conditions are fulfilled:

- in the vacuum space in front of the DI toner assembly (∂G_i denotes the boundary of G_i)

$$\begin{array}{ll} \Delta u_1 = 0, & \mathbf{x} \in G_1, \\ u_1 = 0, & \mathbf{x} \in C_d, \\ u_1 = 0, & \mathbf{x} \in \partial G_1 \cap (\partial G_3 \cup ... \cup \partial G_n), \\ \dfrac{\partial u_1}{\partial n} = \varepsilon_2 \dfrac{\partial u_2}{\partial n}, & \mathbf{x} \in \partial G_1 \cap \partial G_2, \\ \dfrac{\partial u_1}{\partial n} = 0, & \mathbf{x} \in C_l \cap \partial G_1; \end{array} \tag{6.3}$$

- in the dielectric layer on the DI-drum

$$\begin{aligned} &\Delta u_2 = 0, && \mathbf{x} \in G_2, \\ &u_2 = V, && \mathbf{x} \in C_u, \\ &\varepsilon_2 \frac{\partial u_2}{\partial n} = \frac{\partial u_1}{\partial n}, && \mathbf{x} \in \partial G_2 \cap \partial G_1, \\ &\frac{\partial u_2}{\partial n} = 0, && \mathbf{x} \in C_r \cap \partial G_2, \\ &\frac{\partial u_2}{\partial n} = 0, && \mathbf{x} \in C_l \cap \partial G_2; \end{aligned} \tag{6.4}$$

- in the DI toner assembly

$$u_i = 0, \qquad \mathbf{x} \in G_i, \qquad i = 3, \ldots, n. \tag{6.5}$$

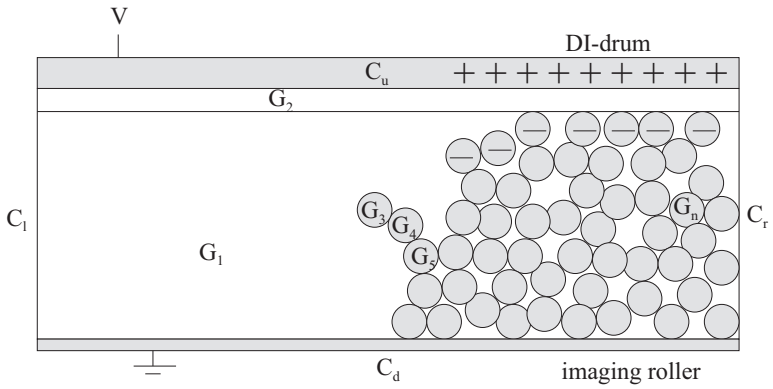

Figure7. The electrostatic problems (6.3)-(6.5) are defined in the depicted front region of the DI toner assembly. The materials depicted in grey are conducting.

Due to the high density of the toner particles in the DI toner assembly, electric screening takes place [13]. A toner particle that is completely surrounded by other toner particles, is screened from the electric field of the DI-drum. This is the reason why charge will only gather at the outer particles of the DI toner assembly that are most near the DI drum. Only these particles will experience an electric force to the DI-drum, and can be printed; see Figure 7.

If the bulk of the DI toner assembly behind the front region is considered as a continuous medium, see Figure 8, the electrostatic problem in the bulk of the DI toner assembly reduces to a Laplace problem for the electric potential u_2 in the dielectric layer, G_2, on the DI drum, of thickness d_l and relative dielectric constant ε_2; that is (x, y as in Figure 8)

$$\begin{aligned} &\Delta u_2(x,y) = 0, && (x,y) \in G_2, \\ &u_2(x,0) = 0, \\ &u_2(x,d_l) = V, \\ &\frac{\partial u_2}{\partial x}(x,y) = 0, && x \to \pm\infty, \end{aligned} \tag{6.6}$$

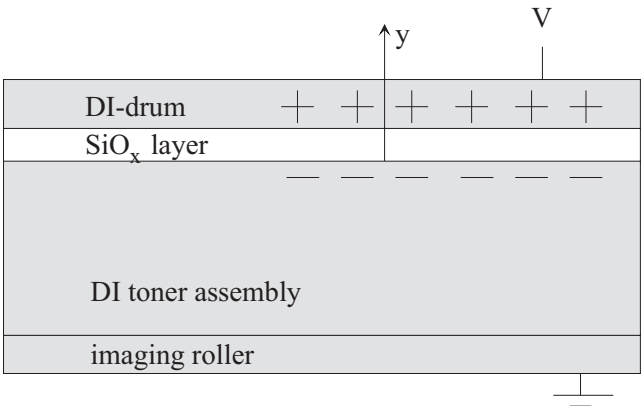

Figure8. The bulk of the DI toner assembly considered as a continuous conducting medium.

with V the prescribed potential of the conducting track of the DI-drum. The solution of (6.6) is

$$u_2(x,y) = V\frac{y}{d_l}. \tag{6.7}$$

From (6.7), the electric surface (line) charge density σ (in C/m) at the boundary $y = 0$, and the electric field strength $\mathbf{E}_2$ in the layer, G_2, can be calculated as

$$\sigma = -\varepsilon_2\varepsilon_0\frac{\partial u_2}{\partial n} = -\varepsilon_2\varepsilon_0\frac{V}{d_l}, \qquad \mathbf{E}_2 = -\nabla u_2 = -\frac{V}{d_l}\mathbf{e}_y. \tag{6.8}$$

The electrostatic force $\mathbf{F}$ acting on a toner particle near the DI drum, in the bulk behind the front region, is (S_p is the average area of that particle in the x, y-plane)

$$\mathbf{F} = \int_{S_p} \sigma(\mathbf{x})\mathbf{E}_2(\mathbf{x})dS. \tag{6.9}$$

The average area occupied by one toner particle is denoted by αR^2. In the case of a dense sphere packing, $\alpha = 2\sqrt{3}$.
Thus, the electrostatic force on one toner particle is given by

$$\mathbf{F} = \frac{\varepsilon_2\varepsilon_0\alpha R^2V^2}{d_l^2}\mathbf{e}_y. \tag{6.10}$$

This formula for $\mathbf{F}$ is specifically valid for a toner particle in the bulk of the DI toner assembly behind the front region that is in contact with the DI drum. This formula will be used for our DEM simulation for the motion of the bulk particles.

For the calculation of the electrostatic force in the front region of the DI toner assembly, we need the electric field strength due a conducting particle in the neighborhood of another conducting particle or a dielectric half-space. In literature, a number of models are described that predict the electric field strength due to a conducting particle in such a situation. Here, the approach of [14,15,16] is adopted, in which bispherical coordinates are used to solve the electrostatic problem for a conducting toner particle in the field of an electrode.

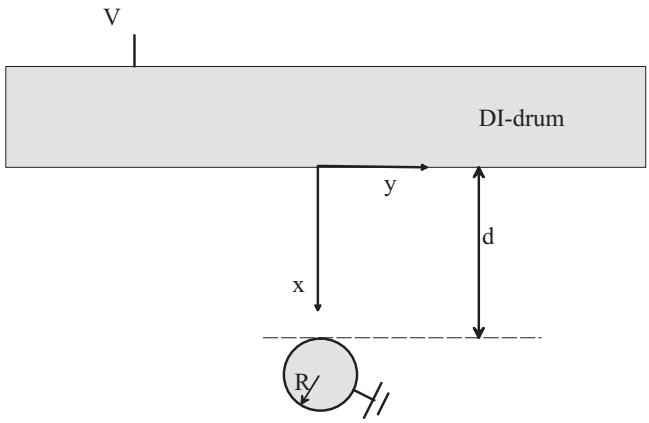

Figure9. A grounded sphere at a distance d from a plate on voltage V.

A grounded sphere of radius R at a distance d from a plate on a voltage V is considered; see Figure 9. The bispherical coordinates ξ, η, ϕ are defined by

$$\begin{aligned} x &= \frac{a \sinh \eta}{\cosh \eta - \cos \xi}, \\ y &= \frac{a \sin \xi \cos \phi}{\cosh \eta - \cos \xi}, \\ z &= \frac{a \sin \xi \sin \phi}{\cosh \eta - \cos \xi}. \end{aligned} \tag{6.11}$$

In terms of these coordinates, the plane $x = 0$, the surface of the plate, is described by $\eta = 0$, and the surface of the sphere by $\eta = \eta_0$, with $\sinh \eta_0 = a/R$, and $a = \sqrt{(d + 2R)d}$. In bispherical coordinates, the Laplace operator applied to the potential u reads

$$\begin{aligned} \nabla^2 u = \frac{(\cosh \eta - \cos \xi)^2}{a^2 \sin \xi} \left\{ \frac{\partial}{\partial \eta} \left(\frac{\sin \xi}{\cosh \eta - \cos \xi} \frac{\partial u}{\partial \eta} \right) + \frac{\partial}{\partial \xi} \left(\frac{\sin \xi}{\cosh \eta - \cos \xi} \frac{\partial u}{\partial \xi} \right) + \right. \\ \left. + \frac{\partial}{\partial \phi} \left(\frac{1}{\cosh \eta - \cos \xi} \frac{\partial u}{\partial \phi} \right) \right\}. \end{aligned} \tag{6.12}$$

The problem, associated to Figure 9, is rotationally symmetric, hence, independent of ϕ. This means that the potential $u = u(\xi, \eta)$, while the problem region is the 2-D region G, with

$$G = \{(\xi, \eta) | 0 < \xi < \pi, 0 < \eta < \eta_0\}. \tag{6.13}$$

The boundary of G is given by $\{\xi = \pi, 0 < \eta < \eta_0\}$, $\{0 < \xi < \pi, \eta = \eta_0\}$, $\{\xi = 0, 0 < \eta < \eta_0\}$, $\{0 < \xi < \pi, \eta = 0\}$, and $\{\xi = 0, \eta = 0\}$ (the latter corresponding with $\sqrt{x^2 + y^2} \to \infty$). The problem for the potential $u^*(\xi, \eta) = u(\xi, \eta) - V$ is then given by

$$\begin{aligned} &\nabla^2 u^* = 0, && (\xi, \eta) \in G, \\ &u^* = 0, && 0 < \xi < \pi, \eta = 0, \\ &u^* = -V, && 0 < \xi < \pi, \eta = \eta_0, \\ &\frac{\partial u^*}{\partial \xi} = 0, && \{\xi = 0 \vee \xi = \pi\}, 0 < \eta < \eta_0, \\ &u^* \to 0, && \xi = 0, \eta = 0 \ . \end{aligned} \tag{6.14}$$

From now on, the superscript in u^* will be omitted. If the Ansatz:
$u(\xi,\eta) = (\cosh\eta - \cos\xi)^{\frac{1}{2}} V_1(\xi)V_2(\eta)$, is used, (6.12) can, after some calculations, be written as

$$\nabla^2 u = \frac{\sin\xi}{(\cosh\eta - \cos\xi)^{\frac{1}{2}}}\left[V_1V_2'' + V_1''V_2 + \frac{\cos\xi}{\sin\xi}V_1'V_2 - \frac{1}{4}V_1V_2\right]. \tag{6.15}$$

Introduction of the separation constant p leads to

$$\begin{aligned} &V_1''(\xi) + \frac{\cos\xi}{\sin\xi}V_1'(\xi) + pV_1(\xi) = 0, \\ &V_2''(\eta) - (\frac{1}{4} + p)V_2(\eta) = 0. \end{aligned} \tag{6.16}$$

First, $(6.16)_1$ will be analyzed. Substitution of $z = \cos\xi$ gives

$$(1-z^2)\frac{d^2V_1}{dz^2} - 2z\frac{dV_1}{dz} + pV_1 = 0. \tag{6.17}$$

This is the differential equation of Legendre [10]. The only solutions of (6.16) that are finite in the domain $-1 \le z \le 1$ are the Legendre Polynomials $P_n(z)$ for $p = n(n+1)$, $n = 0, 1, 2, \ldots$. The fundamental solutions of $(6.16)_2$ are $\cosh(n+\frac{1}{2})\eta$ and $\sinh(n+\frac{1}{2})\eta$. Therefore, a solution of (6.14) in the form

$$u(\xi,\eta) = (\cosh\eta - \cos\xi)^{\frac{1}{2}} \sum_{n=0}^{\infty}\left[a_n\cosh(n+\frac{1}{2})\eta + b_n\sinh(n+\frac{1}{2})\eta\right]P_n(\cos\xi), \tag{6.18}$$

is proposed. From $(6.14)_2$ it follows that $a_n = 0$ for all n. Moreover, since this representation is even, both around $\xi = 0$ and $\xi = \pi$, the condition $(6.14)_4$ is trivially satisfied and, further, this solution also satisfies the condition at infinity $(6.14)_5$. Finally, boundary condition $(6.14)_3$ gives

$$(\cosh\eta_0 - \cos\xi)^{\frac{1}{2}} \sum_{n=0}^{\infty} b_n \sinh\left((n+\frac{1}{2})\eta_0\right)P_n(\cos\xi) = -V\ , \tag{6.19}$$

a relationship for the still unknown coefficients b_n. This relation renders (for $-1 < z = \cos\xi < 1$)

$$\begin{aligned} \sum_{n=0}^{\infty} b_n \sinh\left((n+\frac{1}{2})\eta_0\right)P_n(z) &= -\frac{V}{(\cosh\eta_0 - z)^{\frac{1}{2}}} = -\frac{V\sqrt{2}}{e^{\frac{\eta_0}{2}}\sqrt{1 + e^{-2\eta_0} - 2ze^{\eta_0}}} \\ &= -V\sqrt{2}\sum_{n=0}^{\infty} e^{-(n+\frac{1}{2})\eta_0}P_n(z), \end{aligned} \tag{6.20}$$

and then the orthogonality of the Legendre polynomials yields

$$b_n = -\frac{V\sqrt{2}e^{-(n+\frac{1}{2})\eta_0}}{\sinh(n+\frac{1}{2})\eta_0}\ . \tag{6.21}$$

Hence, the solution of (6.14) is given by

$$u = -V\sqrt{2}(\cosh\eta - \cos\xi)^{\frac{1}{2}} \sum_{n=0}^{\infty} e^{-(n+\frac{1}{2})\eta_0}\frac{\sinh(n+\frac{1}{2})\eta}{\sinh(n+\frac{1}{2})\eta_0}P_n(\cos\xi). \tag{6.22}$$

Note that the series in this solution converge for $d > 0$ (or $\eta_0 > 0$) for all $(\xi, \eta) \in G$.

The electrostatic force F on the sphere is directed towards the plane $x = 0$, and, according to (6.1), this force is given by (with $G \in \mathbb{R}^3$ replaced by $S \in \mathbb{R}^2$, the surface $\eta = \eta_0$ of the sphere)

$$F = -\int_S \sigma E_x dS, \tag{6.23}$$

with

$$\sigma = \varepsilon_0 \frac{\partial u}{\partial n}\bigg|_S = \varepsilon_0 \frac{\cosh\eta_0 - \cos\xi}{a} \frac{\partial u}{\partial \eta}\bigg|_{\eta=\eta_0}, \tag{6.24}$$

and

$$E_x = -\frac{\partial u}{\partial x} = -\frac{\cosh\eta_0 \cos\xi - 1}{a} \frac{\partial u}{\partial \eta}\bigg|_{\eta=\eta_0}. \tag{6.25}$$

Here it has been used that the tangential derivative $\partial u/\partial \xi = 0$ at $\eta = \eta_0$. Finally, for the surface element

$$dS = \frac{a^2 \sin\xi}{(\cosh\eta_0 - \cos\xi)^2} d\xi d\phi, \tag{6.26}$$

holds. All this leads to

$$F = 2\pi\varepsilon_0 \int_0^\pi \frac{(\cosh\eta_0 \cos\xi - 1)\sin\xi}{\cosh\eta_0 - \cos\xi} \left(\frac{\partial u}{\partial \eta}\bigg|_{\eta=\eta_0} \right)^2 d\xi. \tag{6.27}$$

From (6.22), with use of (6.20), we obtain

$$\frac{\partial u}{\partial \eta}\bigg|_{\eta=\eta_0} = -\frac{V\sqrt{2}}{\cosh\eta_0 - \cos\xi} \left(V_1 + V_2\right) \ , \tag{6.28}$$

with ($z = \cos\xi$)

$$\begin{aligned} V_1 &= \frac{\sinh\eta_0}{2\sqrt{2}}, \\ V_2(z) &= (\cosh\eta_0 - z)^{3/2} \sum_{n=0}^{\infty} \left(n + \frac{1}{2}\right) \frac{\cosh(n+\frac{1}{2})\eta_0}{\sinh(n+\frac{1}{2})\eta_0} e^{-(n+\frac{1}{2})\eta_0} P_n(z). \end{aligned} \tag{6.29}$$

With (6.28), the expression on the right-hand side of (6.27) can be split up in three separate integrals

$$F = 4\pi\varepsilon_0 V^2 (F_1 + F_2 + F_3), \tag{6.30}$$

with

$$\begin{aligned} F_1 &= V_1^2 \int_{-1}^{1} \frac{x\cosh\eta_0 - 1}{(\cosh\eta_0 - x)^3} dx, [0.3cm] \\ F_2 &= 2V_1 \int_{-1}^{1} V_2 \frac{x\cosh\eta_0 - 1}{(\cosh\eta_0 - x)^3} dx, [0.3cm] \\ F_3 &= \int_{-1}^{1} V_2^2 \frac{x\cosh\eta_0 - 1}{(\cosh\eta_0 - x)^3} dx. \end{aligned} \tag{6.31}$$

Evaluation of the integral F_1 results in

$$F_1 = 0. \tag{6.32}$$

The integral F_2 can be rewritten as

$$F_2 = 2V_1 \sum_{n=0}^{\infty} v_n \int_{-1}^{1} \frac{z\cosh\eta_0 - 1}{(\cosh\eta_0 - z)^{3/2}} P_n(z)dz, \tag{6.33}$$

with

$$v_n = \left(n + \frac{1}{2}\right) \frac{\cosh(n+\frac{1}{2})\eta_0}{\sinh(n+\frac{1}{2})\eta_0} e^{-(n+\frac{1}{2})\eta_0}. \tag{6.34}$$

With the introduction of the auxiliary function J_n as

$$J_n(\cosh\eta_0) = \int_{-1}^{1} \frac{P_n(z)}{\sqrt{\cosh\eta_0 - z}} dz = \frac{2\sqrt{2}}{2n+1} e^{-(n+\frac{1}{2})\eta_0} \ , \tag{6.35}$$

which is such that ($\zeta = \cosh\eta_0$)

$$\int_{-1}^{1} \frac{z\zeta - 1}{(\zeta - z)^{3/2}} P_n(z)dz = -\zeta J_n(\zeta) - 2(\zeta^2 - 1)J_n'(\zeta) \ , \tag{6.36}$$

the right-hand side of (6.33) can be evaluated to

$$F_2 = \sum_{n=0}^{\infty} \frac{\cosh(n+\frac{1}{2})\eta_0}{\sinh(n+\frac{1}{2})\eta_0} e^{-(2n+1)\eta_0} \sinh\eta_0 \left(ne^{\eta_0} - (n+1)e^{-\eta_0}\right). \tag{6.37}$$

The integral F_3 can be calculated straightforwardly, giving

$$\begin{aligned} F_3 = &\sum_{n=0}^{\infty} \frac{\cosh(n+\frac{1}{2})\eta_0}{\sinh(n+\frac{1}{2})\eta_0} e^{-(n+\frac{1}{2})\eta_0}. \\ &\cdot \left[-(n+\frac{1}{2}) \frac{\cosh(n+\frac{1}{2})\eta_0}{\sinh(n+\frac{1}{2})\eta_0} e^{-(n+\frac{1}{2})\eta_0} + (n+1)\cosh\eta_0 \frac{\cosh(n+3/2)\eta_0}{\sinh(n+3/2)\eta_0} e^{-(n+3/2)\eta_0} \right]. \end{aligned} \tag{6.38}$$

With this result, an explicit expression for the Coulomb force on one earthed spherical particle at a distance d (related to η_0) from a plate on voltage V has been obtained. This formula will be used in our DEM simulations for front-region particles.

The DI-drum consists of a number of conducting tracks, which separately can be put on a voltage. When a pixel has to be printed, a voltage difference is applied between the imaging roller and a track in the DI-drum. This voltage difference causes toner particles in the DI toner assembly to get charged and to experience an electric force towards the DI-drum that is stronger than the magnetic force towards the imaging roller. An SiO_x layer, the dielectric layer above the conducting tracks, ensures that the electric charge on the toner does not leak to the conducting tracks. This way, toner particles stay on the DI-drum. In the clean situation, when nothing has to be printed, the voltage difference between the imaging roller and the track of the DI-drum is put off. In this stage, the charge of the toner in the DI toner assembly leaks to the imaging roller, the toner does not experience an electric force any more and is

pulled from the DI-drum by the magnetic force of the magnet within the imaging roller. Due to the charging and decharging of the DI toner assembly, the voltage difference between toner particles and the DI-drum changes in time, and, according to (6.30), the electric force does.

Due to the dynamics of the DI toner assembly, conducting paths are formed and broken. The conducting paths consist of toner-toner contacts and toner-imaging roller contacts. We treat the contact between a toner particle and another toner particle as an ideal electric resistance. Similarly, the contact between a toner particle and the imaging roller is treated as an ideal electric resistance. A toner particle that approaches the DI-drum builds up charge and an electric force towards the DI-drum. Toner particles within a small range of the DI-drum are treated as a capacitor with respect to the DI-drum. Particles in contact with the DI-drum build up charge, and have some charge leakage into the DI-drum. The contact of a toner particle with the DI-drum is treated as a capacitor in parallel with an ideal resistance. By this routine, a simulation geometry can be transferred into an electric circuit. Several methods [17] are available to analyze a resistive network. Our approach consists of a 1-dimensional analysis of the electric circuit. We assume that the charging of toner particles is mainly due to a flow of charge through the shortest conductive path formed to the imaging roller. This shortest path is calculated for every particle and is translated to a 1-dimensional electric circuit. The computational costs of this approach are limited, so that the method can be applied in a discrete element method simulation. Furthermore, the relevant physics that play a role in the charging process is captured in this method: charging of a particle in contact with a charged object takes place according to an RC-time, and particles cannot be charged or decharged if they are not in conducting contact with the imaging roller. This means that charge can only be distributed during collisions of particles that form conducting chains to the imaging roller.

7 Validation and results

Print quality is a global concept, covering a lot of areas such as detail reproduction, graininess, and color gamut. Two main determinants of color print quality are resolution, measured in dots per inch (dpi), and the number of levels or graduations that can be printed per dot. Generally speaking, the higher the resolution and the more levels per dot, the better the overall print quality. In practice, most printers make a trade-off, some opting for higher resolution and others settling for more levels per dot, the best solution depending on the printer's intended use.

The edges of printed dots are in general not perfectly sharp. The front edge, the beginning of a pixel, and the back edge, the end of a pixel, are not perfect, but have a certain edge sharpness. Unsharp edges in the direction of a ring electrode of the DI-drum occur because switching the print voltage on and off does not immediately imply a transition of toner coverage from 0% to 100% or vice versa. Edge sharpness is defined as the distance in micrometers over which the coverage in an edge changes from 10% to 90%, where the maximum coverage in a pixel is scaled to 100%. Big dots consist of a front edge, a middle part where the toner coverage is maximal and stable, and a back edge. Small dots only consist of a front edge and a back edge, without a middle part. Edge sharpness thus contains information of the stability and quality with which pixels or dots can be printed by a development unit, and is thus an important print quality measure for a development unit. Consequently, if we are able to predict edge sharpness with our DEM simulation tool, we can predict aspects of print

quality of a full color engine. Here, we investigate to what extent we are able to predict edge sharpness of printed dots for a black DI-unit of the Océ CPS700.

In order to determine edge sharpness from DEM simulations, we run a total number of fifty simulations, where in each simulation a line is printed. In Figure 10, the result of one of these fifty simulations is displayed. Each single printed line contains an edge sharpness.

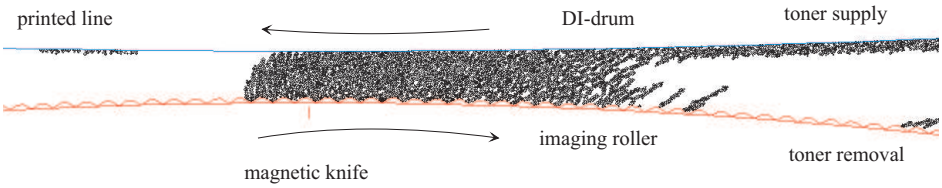

Figure10. Snapshot of a DEM simulation movie of the black unit of the Océ CPS700. A line has been printed on the upper drum, the DI-drum. The lower drum is the imaging roller. The imaging roller has a mechanical roughness (dredger profile) and a magnetic knife placed underneath.

Different printed lines put next to each other show a non-perfect edge sharpness due to a shift in the area of full coverage. Both effects are accounted for by determining an average coverage curve from the fifty printed lines. The average coverage curve is determined by averaging the individual coverage curves from the fifty simulations. The individual coverage curves simply depict the presence (defined as 100% coverage) or absence (defined as 0% coverage) of toner on the DI-drum as a function of the position on the DI-drum. From the average coverage curve, a sigmoid fit is calculated; sigmoid fits are predefined functions, which are part of a standard measurement protocol to determine edge sharpness of printed dots. From the sigmoid fit, the normal front and back edge sharpness can be determined. The coverage profiles, determined by experiments or by simulations, for a black unit of the Océ CPS700 are displayed in Figure 11. Good quantitative agreement is observed between the simulation and the experimental results. Both simulation and experimental results show an a-symmetry: the back edge sharpness is better than the front edge sharpness.

This not only confirms us in the quality of the model, but also opens opportunities for many applications of the model. The model can, for instance, be used to predict aspects of print quality for deviating settings of the DI-unit. Since it is relatively easy to do predictions with the DEM model for exotic settings of the DI-unit, new ideas can be tested fast and good ideas discovered more easily. The model can also be used as a design tool for fundamentally new ideas, which are difficult to test experimentally. Furthermore, the DEM model provides a lot of insight in the relevant processes that take place in the DI toner assembly, and allows people to improve the system on basis of a fundamental insight in the physics playing a role in the development process.

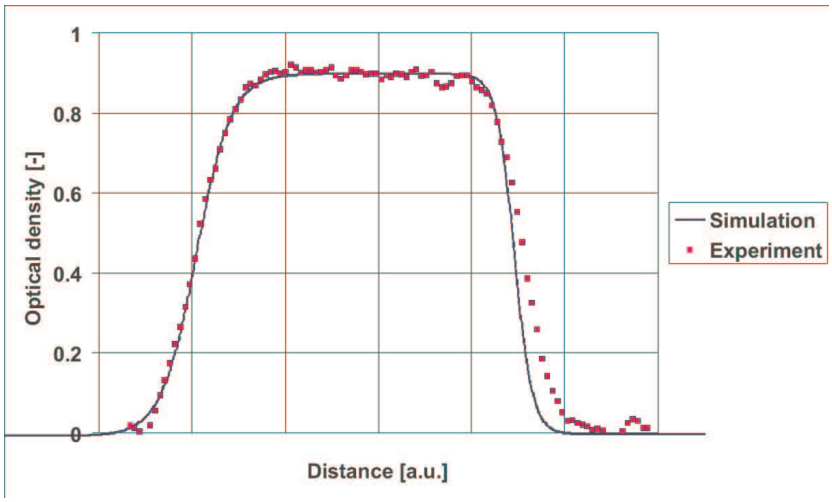

Figure11. The coverage profiles determined by experiments or by simulations for a black unit of the Océ CPS700.

References

1. Severens, I.E.M., *DEM simulations of toner behavior in the development nip of the Océ Direct Imaging print process*, PhD thesis, Eindhoven University of Technology, (2005).
2. Severens, I.E.M. and Ven, A.A.F. van de, *DEM simulations of toner behavior in the development nip of the Océ Direct Imaging print process*, In: Proceedings of the XIVth International Symposium on Trends in Applications of Mathematics to Mechanics (STAMM04), Seeheim, Germany, 22-28 August 2004, pp. 483-492. Eds.: Y. Wang and K. Hutter, Shaker Verlag, Aachen (2005).
3. Cundall, P.A., *A computer model for simulating progressive large-scale movements in block rock systems*, Proc. Symp. Int. Soc. Rock Mech. **2**, (1971).
4. Cundall, P.A. and Strack, O.D.L, *A discrete numerical model for granular assemblies*, Géotechnique **29**, 47 (1979).
5. Haff, P.K. and Werner, B.T., *Computer simulation of the mechanical sorting of grains*, Powder Technol. **48**, 239 (1986).
6. Wolf, D.E., *Modelling and computer simulation of granular media*, Computational Physics, 64-94 (1996)
7. Severens, I.E.M., Mattheij, R.M.M., Wolf, D.E., and Ven, A.A.F. van de, *Parameter estimation and validation of DEM simulations of a print process*, forthcoming.
8. Hamaker, H.C., *The London-Van der Waals attraction between spherical particles*, Physica **4**, 1058 (1937).
9. Stratton, J.A., *Electromagnetic Theory*, McGraw-Hill, New York, (1941).
10. Arfken, G., *Mathematical Methods for Physicists*, Academic Press, 637-711 (1985).
11. Jackson, J.D., *Classical Electrodynamics*, John Wiley & Sons, New York (1999).
12. CEDRAT, *Flux2D*, http://www.cedrat.com.
13. Smythe, W.R., *Static and dynamic electricity*, McGraw-Hill book company, New York (1950).
14. Warren, W.E. and Cuthrell, R.E., *Electrostatic forces between conducting spheres at constant potential*, Journal of Applied Physics **46**, 4597-4599 (1975).

15. Berry, J.S., *Electrostatic forces on a conducting sphere due to a charge on a dielectric half-space*, J. Phys. A: Math. Gen **9**, 1939-1945 (1976).

16. Lapiga, E.Ya. and Loginov, V.I., *Strength of electric field in gap between two charged, conductive, spherical particles*, Plenum publishing, 760-767 (1990).

17. Rizzoni, G., *Principles and Applications of Electrical Engineering*, McGraw-Hill, New York (2003).